Pergamon

Cement and Concrete Research 31 (2001) 993–1001

CEMENT AND CONCRETE RESEARCH

^{29}Si and ^{27}Al high-resolution NMR characterization of calcium silicate hydrate phases in activated blast-furnace slag pastes

J. Schneider[a,*], M.A. Cincotto[b], H. Panepucci[a]

[a]*Instituto de Física de São Carlos, Universidade de São Paulo, Av. Carlos Botelho 1465, Caixa Postal 369, CEP 13560-970, São Carlos, SP, Brazil*
[b]*Departamento de Engenharia de Construção Civil, PCC/EPUSP, Universidade de São Paulo, Caixa Postal 61.548, São Paulo, SP 05424-970, Brazil*

Received 20 September 1999; accepted 25 April 2001

Abstract

Within the framework of improving mechanical properties of activated blast-furnace slag cements, a set of hardened pastes of 28 days age were analyzed by ^{29}Si and ^{27}Al high-resolution nuclear magnetic resonance (NMR) at 9.4 T. Structural and compositional differences among C-S-H phases obtained with different activation and curing conditions were characterized by NMR. Activation of the slag was done with compounds of different alkalinity (sodium silicate, sodium hydroxide, calcium hydroxide and gypsum), and under steam and wet curing. Parameters characterizing the extent of the hydration reaction, the polymerization degree of the aluminum-silicate chains and the Al/Si ratio in C-S-H were obtained from NMR spectra. ^{29}Si-NMR spectra indicated that connectivites of silicate tetrahedra in all pastes are compatible with the "dreierkette" structural model of C-S-H. A substantial degree of polymerization of the aluminum-silicate groups in C-S-H was observed in pastes resulting from activation with sodium silicate and gypsum/calcium hydroxide blend. Steam curing and a higher alkali concentration enhanced the incorporation of Al in C-S-H. Even with low concentration of alkali, through steam curing it is possible to obtain a degree of incorporation of Al in C-S-H as high as in the case of higher alkali addition.

Keywords: Granulated blast-furnace slag; Calcium-silicate-hydrate (C-S-H); NMR spectroscopy; Thermal treatment

1. Introduction

Granulated blast-furnace slag (gbfs) cements are interesting materials in order to produce fiber-reinforced cementitious matrices. Low alkalinity gbfs cements can be used in structures reinforced with low-cost glass and vegetal fibers [1]. Though alkali activation of gbfs is the most efficient way to obtain high mechanical strength cements, the combination of low contents of alkali activators and adequate steam curing can also accelerate the hydration reaction, assuring high strength at early ages [2–6].

Calcium silicate hydrate (C-S-H) is the main binding agent in cements. Its structural characterization is a key point in order to improve basic understanding of how activators and cure influence the properties of the final product. For this purpose, high-resolution nuclear magnetic resonance (NMR) is a suitable characterization tool for both the amorphous and poorly crystalline phases present in hardened pastes. Short- and medium-range order can be locally probed by NMR, complementing the information about long range periodicities provided by X-ray diffraction. The extent of the hydration reaction, the polymerization degree of the aluminum-silicate chains and the extent of incorporation of Al into the C-S-H can be obtained from the ^{29}Si-NMR spectra. Also, ^{27}Al-NMR can be used to discriminate Al atoms in tetrahedral or octahedral coordination, as they respectively appear in C-S-H and in other hydrated phases present in hardened pastes. The technique of cross-polarization NMR (CP) from the system of ^{1}H to X nuclei (where X is, for example, ^{29}Si or ^{27}Al) is another helpful tool, which provides spectra only from those X nuclei spatially close to ^{1}H, typically less than 5 Å.

As part of a study to optimize the mechanical properties of low alkalinity gbfs cements, several hardened pastes were characterized by high-resolution NMR methods. In previous NMR studies of this kind of cements, the activation with sodium hydroxide (NaOH) and potassium hydroxide (KOH) were considered [7,8]. In those cases, the experimental data supported the "dreierkette" structural models of C-S-H.

* Corresponding author. Tel.: +55-16-273-9600; fax: +55-16-273-9876.
E-mail address: schnei@if.sc.usp.br (J. Schneider).

0008-8846/01/$ – see front matter
PII: S0008-8846(01)00530-0

Table 1
Composition of the commercial gbfs

Oxide	Weight (%)	Oxide	Weight (%)
LOI	1.67	SO_3	0.15
SiO_2	33.78	Na_2O	0.16
Al_2O_3	13.11	K_2O	0.32
FeO	0.23	S^{2-}	1.14
CaO	42.47	CaO free	0.1
MgO	7.46	Insoluble	0.53

Also, information about the silicate organization and the incorporation of aluminum into the C-S-H phase could be obtained [7,8]. In this work, we extend those NMR studies to C-S-H phases obtained from activation of gbfs with several selected compounds of different alkalinity (sodium silicate, sodium hydroxide, calcium hydroxide and gypsum). Steam curing was applied in all pastes, and two alkali-activated pastes (sodium silicate) were wet-cured for the sake of comparison. The structural differences among the C-S-H phases obtained in each paste were characterized by ^{29}Si and ^{27}Al high-resolution NMR. Also, the extent of the reaction was evaluated from ^{29}Si-NMR spectra. Results are discussed in connection with the measured values of mechanical resistance and powder X-ray diffraction information.

2. Experimental procedure

Commercial gbfs (Companhia Siderúrgica de Tubarão, ES, Brazil) was ground in a ball mill until Blaine fineness of 500 m^2/g. Chemical composition of the slag is presented in Table 1. The glass content of the slag was evaluated by optical microscopy as 99.5%. The gbfs pastes were prepared with different activators, as indicated in Table 2, with water/solid ratio of 0.48 and sealed in cylindrical tubes (35 mm diameter, 50 mm height) for curing. Two kinds of cure were performed in different pastes. Wet curing was carried out at 25°C with relative humidity (RH) greater than 95%. Steam curing (RH > 95%) parameters are indicated in Table 2. The thermal cycle (rising, stabilization at maximum temperature and cooling to room temperature) was applied after a wait time at room temperature, dependent on the activator. This time was chosen as the time of initial setting of each cement, previously determined at 25°C by isothermal calorimetric measurements. In all steam curing processes, the heating and cooling gradients were 30°C/h. After 28 days the hydration reactions were quenched. Slices of 2 mm maximum thickness were cut from the cylinders, immersed in anhydrous isopropyl alcohol for 10 days and dried under vacuum at 50°C for 18 h. Specimens for NMR and X-ray diffraction were finely ground to powder. X-ray diffractometry was performed in a Phillips MPD180 apparatus. Figs. 1 and 2 show the diffraction patterns. From these data, the presence of C-S-H, CAH_{10}, C_3AH_6 and CH phases in the set of samples can be detected. Samples P5 and P7 show the greatest content of CAH_{10} and perhaps some amount of AFm phases as $C_4(A,F)H_{13}$. Instead, sample P6 shows a substantial amount of ettringite and traces of activators (calcium hydroxide and gypsum).

Cylindrical samples (50 mm diameter, 100 mm height) were cast from mortar 1:3:0.48 (cement/sand/water based on mass) and were tested for compressive strength at 28 days with load speed of 60 N/s. Strength results are shown in Table 4. The standard deviation values of these determinations were less than 2 MPa.

High-resolution ^{29}Si-NMR spectra were obtained at a frequency of 79.45 MHz (9.4 T) with a Varian Unity INOVA spectrometer. Measurements were carried out under Magic Angle Sample Spinning (MAS) up to 5 kHz in zirconia rotors with a Varian 7 mm wide-body probe. The spectra were obtained from Bloch Decay (BD) signals after $\pi/2$ pulses of 4 μs length with 30 s recycle time and collecting up to 3000 free induction decay (FID) signals. No differential saturation effects were observed with this repetition rate, enabling the quantitative comparison of intensities for each spectrum. Kaolinite was used as secondary external standard for chemical shift (-91.2 ppm with respect to TMS).

^{27}Al-NMR-MAS spectra were obtained at 104.22 MHz with the same spectrometer and probe, using BD and ^{1}H–^{27}Al CP techniques, with high power ^{1}H decoupling. In BD experiments, radio frequency pulses of 1 μs, corresponding to 20° tip angle, were used in order to excite all quadrupole transitions in ^{27}Al. In CP experiments, $\pi/2$ pulses for ^{1}H of 4 μs were applied. The contact time for

Table 2
Activator compound and curing parameters of the gbfs pastes

Paste	Activator		Cure	Maximum cure temperature [°C]	Waiting time [h]
	Compound	Weight content			
P1	Sodium silicate	1.85%Na_2O; 3.15%SiO_2	Wet	25	–
P2	Sodium silicate	5%Na_2O; 8.5%SiO_2	Wet	25	–
P3	Sodium silicate	1.85%Na_2O; 3.15%SiO_2	Steam	60	17
P4	Sodium silicate	5%Na_2O; 8.5%SiO_2	Steam	60	3.5
P5	Calcium hydroxide	5%	Steam	60	5
P6	Calcium hydroxide + gypsum	2%$Ca(OH)_2$ + 6%$CaSO_42H_2O$	Steam	60	3
P7	Sodium hydroxide	Equivalent to 5% Na_2O	Steam	60	0.75

Aging time: 28 days.

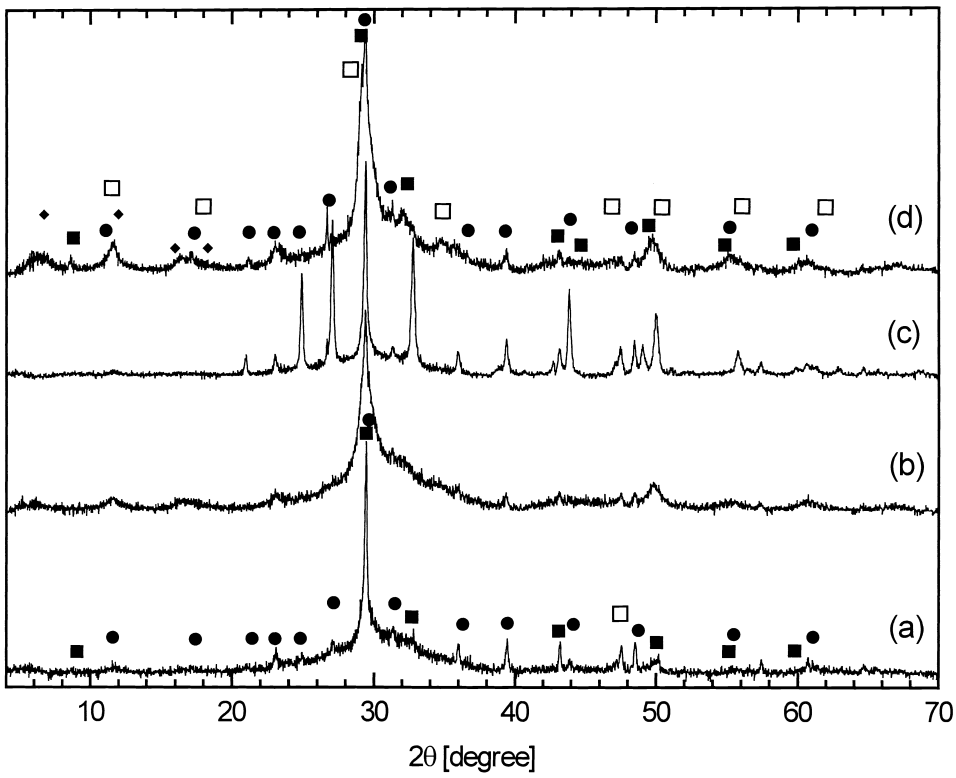

Fig. 1. X-ray diffraction patterns from alkali-activated hydrated pastes (a) P1, (b) P2, (c) P3 and (d) P4. ■ = C-S-H, ◆ = CAH_{10}. ● = C_3AH_6, □ = CH. For clarity, the symbols are not superimposed to all diffraction patterns.

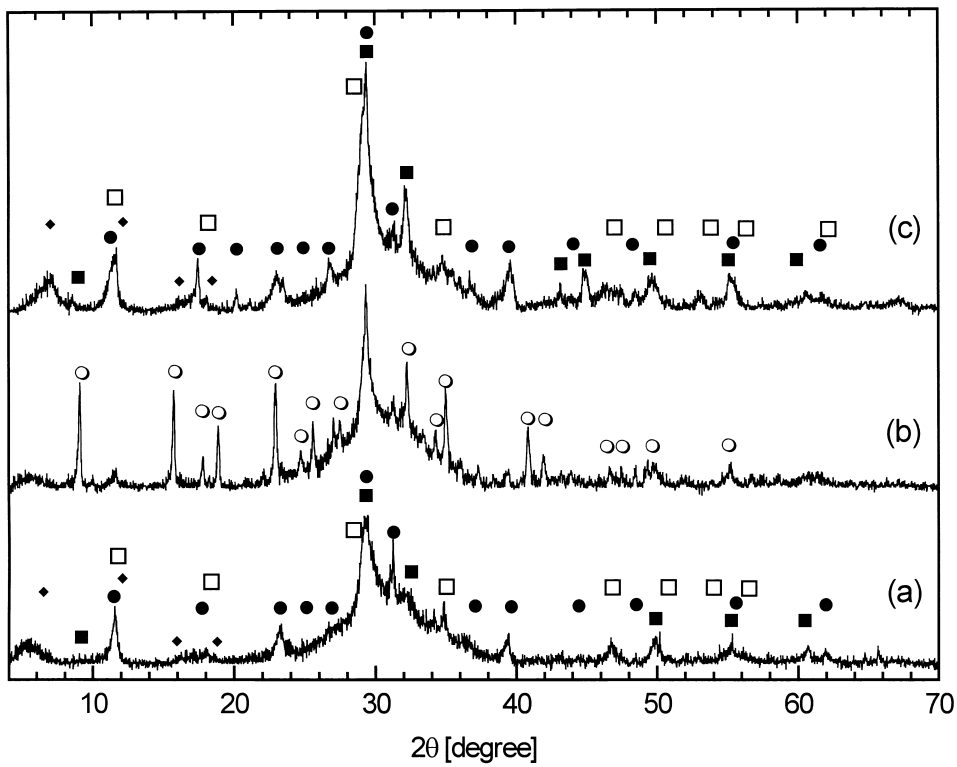

Fig. 2. X-ray diffraction patterns from hydrated pastes (a) P5, (b) P6, and (c) P7. ■ = C-S-H, ◆ = CAH_{10}. ● = C_3AH_6, □ = CH, ○ = ettringite. For clarity, the symbols are not superimposed to all diffraction patterns.

maximum signal intensities was determined as 300 μs. Recycle times of 5 s were used in both kinds of experiments and approximately 1000 FID's were collected. Phase cycling was applied in all pulse sequences, especially in ^{27}Al-CP experiments in order to avoid non-CP spurious signals [9]. The Hartmann–Hahn match condition for ^{1}H–^{27}Al CP was adjusted with a sample of kaolinite. ^{27}Al chemical shifts were referenced to an external standard of 0.1 M $Al_2(SO_4)_3$, with accuracy better than ±1 ppm.

3. Results

3.1. ^{29}Si-NMR spectroscopy

Fig. 3 shows the ^{29}Si-NMR spectra of the gbfs and the hydrated pastes. The gbfs sample shows a single broad resonance centered at −74.5 ppm. The gaussian-like profile and the high value of half height line width (11.5 ppm) are a consequence of the glassy structure of the slag. The central value of the observed chemical shift distribution in gbfs indicates that silicate groups are mostly organized in Q^1 dimeric units [10]. According to widespread use, SiO_4^{4-} units are identified according to their mutual connectivity as $Q^n(m\mathrm{Al})$, where n is the number of shared oxygen atoms with other silicate or aluminate tetrahedra, and m is the number of neighbor aluminate groups.

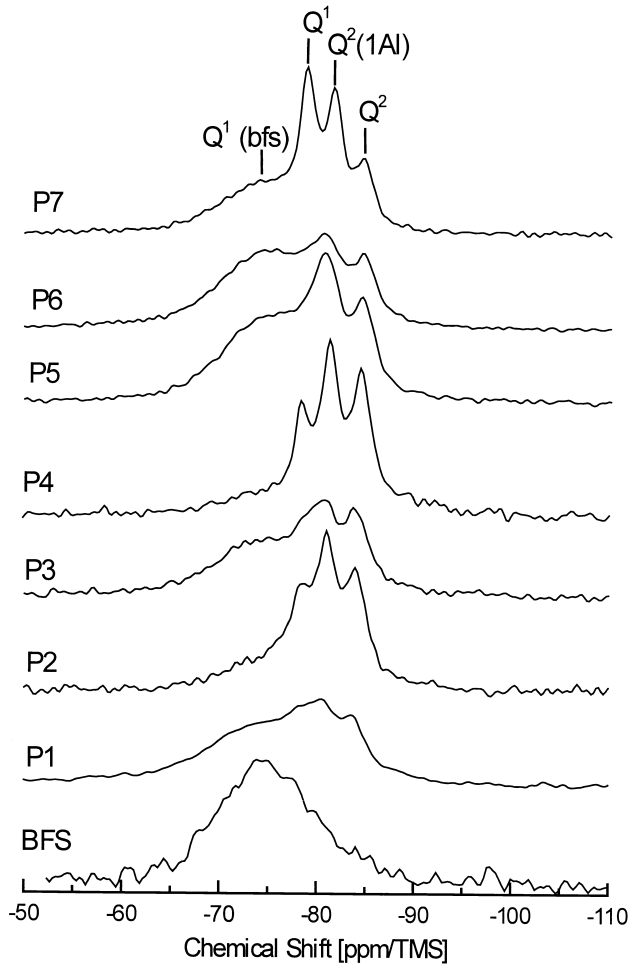

Fig. 3. ^{29}Si-BD-MAS-NMR spectra from gbfs and hydrated pastes. Marks on the peaks show the assignments of resonances with silicon environments.

As seen in Fig. 3, spectra from cement pastes show three easily resolved resonances associated with ^{29}Si in hydration products (mainly C-S-H phase as indicated by the X-ray patterns) in addition to the broad line around −74 ppm corresponding to ^{29}Si in unreacted slag. Also, a weak signal around −90 ppm with less than 2% of the total intensity and more than 6 ppm width could be observed in the spectra of samples P4 and P2. Considering that these samples have the greater sodium content of the set, it is possible that this line corresponds to a small amount of some zeolite phase. However, identification by means of the X-ray diffraction patterns proved to be difficult due to coincidence of some diffraction peaks with other well identified phases. Therefore, if zeolites are present their quantity is small. The weak −90 ppm signals in the ^{29}Si-NMR spectra of P2 and P4 were disregarded in the rest of the analysis.

A deconvolution of the spectra was done using three lorentzian functions for silicon in hydrated products and one gaussian for silicon in gbfs. Table 3 shows the chemical shifts for the resonances obtained from least-square fitting. The fitted half height line-width values were lower than 3 ppm, revealing a better defined chemical environment for ^{29}Si in hydrated products with respect to the slag. These line-widths are typical for ^{29}Si in partially crystalline materials, indicating the higher degree of order of the hydrated phase relative to gbfs. The relative amount of silicon in each kind of Q^n connectivity is directly proportional to the integrated intensities A(Q^n) of the deconvoluted lines in the BD-NMR spectra. Hence, it is possible to evaluate the extent of the hydration reaction for each paste by considering the ^{29}Si intensities of the resonance lines from gbfs and C-S-H. Table 4 shows the percentage r of silicon in C-S-H relative to gbfs, which quantifies the extent of the reaction. The effects of activator and cures can be more easily visualized in the plot of r for each sample, shown in Fig. 4a. The values of compressive strength are also shown in order to keep in mind the mechanical properties of the obtained product. As can be seen, considering the group P1 to P4, higher alkali concentration and steam cure improved the extent of the reaction. The highest values of r in the whole set of pastes correspond to P4 (r = 88%) and P2 (r = 81%), the samples richest in Na_2O (5%). Considering the strength values for these pastes, an improvement of the resistance for pastes with higher Na_2O content was observed (P2 with respect to P1 and P4 with respect to P3). On the other hand, despite the substantial increase of r with the steam cure for P3 and P4, the mechanical resistance of these pastes is lower than in the corresponding wet-cured samples. This fact may be related with the early formation of thick C-S-H outer shells around the silicate grains, limiting the

Table 3
Chemical shifts resulting from the deconvolution of the ^{29}Si-NMR spectra of gbfs and C-S-H pastes and resonance assignments

	gbfs	P1	P2	P3	P4	P5	P6	P7	Description
Gauss	− 74.5	− 74.2	− 74.7	− 74.4	− 73.4	− 74.9	− 74.6	− 74.1	Q^1-gbfs
Lorentz	–	− 78.8	− 78.3	− 79.0	− 78.4	− 80.4	− 80.1	− 78.9	Q^1-C-S-H
Lorentz	–	− 80.7	− 81.0	− 80.8	− 81.2	− 81.3	− 81.4	− 81.7	Q^2(1Al)-C-S-H
Lorentz	–	− 83.7	− 84.0	− 84.0	− 84.6	− 84.8	− 84.9	− 84.8	Q^2-C-S-H

growth of inner shell C-S-H responsible for resistance at subsequent stages. Activation with calcium hydroxide ($Ca(OH)_2$) and NaOH (P5 and P7, respectively) produces similar values of strength, comparable to pastes with 2% Na_2O. Also, a low extent of reaction is measured in these samples. The activation with $Ca(OH)_2$/gypsum blend (P6) gave the poorest values of r in the set. The low mechanical resistance of this specimen may be explained from the low reactivity measured.

From the isotropic chemical shift of the ^{29}Si resonance lines of C-S-H, shown in Table 3, it is possible to identify several kinds of connectivities between aluminum-silicate groups in the gel. Considering literature data [7,10], the resonance lines around − 78, − 81 and − 84 ppm can be assigned, respectively, to silicon in Q^1, Q^2(1Al) and Q^2 groupings. So, disregarding a possibly small amount of zeolite in P2 and P4, the existence of hydrated phases with three-dimensional networks or branching tetrahedra can be excluded in these pastes. Also, Al substitutions in tetrahedral sites are detected only as Q^2(1Al) groupings.

Structural models for C-S-H, applicable to several kinds of cement pastes, have been proposed and analyzed in detail [8,11–13]. In these models, closely related to the 1.4-nm tobermorite structure, silicate groups in C-S-H organize in linear "dreierkette" chains. Silicon vacancies or Al substitutions can occur at special sites of the chain corresponding to tetrahedra not linked to calcium atoms, the so-called bridging tetrahedra. Then, finite chains of alumino-silicate groups result, with aluminate tetrahedra located only between two nonbridging silicate dimers [8,11]. Values for the length of these chains, defined as the number of tetrahedra between two silicon vacancies, result restricted to the sequence 2, 5, 8, 11, … $3n-1$, with n integer. The $Q^n(m\text{Al})$ species observed in the NMR spectra of the hydrated gbfs pastes are compatible with this structural model. In this way, the Q^1 resonance should correspond to silicates forming dimers or located at chain ends. Q^2(1Al) and Q^2 resonances should be associated to chain mid-member silicates, respectively, with and without an Al substituted tetrahedron.

In the framework of the "dreirkette" models, there are two parameters characterizing the structural and compositional features of the C-S-H phase that can be obtained from the integrated intensities of the NMR lines, as shown for example in Ref. [8]. The first one is the mean length of silicate chains (MCL), the average number of tetrahedra between two empty bridging sites [8]. The second one is the content of aluminum substituted in the C-S-H chains with respect to silicon (Al/Si) [8]. The values for MCL and Al/Si obtained for the set of pastes are summarized in Table 4. Previous NMR determinations of MCL in NaOH/KOH-activated slags and Portland cement blends revealed a silicate organization mostly in pentameric units, with some quantity of octamers [7,8,13]. It is interesting to note that substantially higher values of MCL were obtained in some of the pastes studied. As can be inferred from the MCL values shown in Table 4, aluminum-silicates in C-S-H phases of P4, P2 and P6 are highly polymerized, with a substantial amount of chains longer than octamers. In the other pastes, a number of pentamers and octamers should coexist. The values of MCL obtained for each paste are plotted in Fig. 4b in order to visualize the effect of activators and cure type. Pastes activated with higher Na_2O concentrations lead to C-S-H phases with the longest MCL values. Though steam curing clearly favored the development of longer chains in P4 with respect to P2 (both with 5% Na_2O), almost the opposite behavior was verified in P3 with respect to P1 (2% Na_2O). In the case of P6, the C-S-H chains are as long as those found in more hydrated samples. Therefore, the polymerization degree of the

Table 4
Parameters obtained for gbfs pastes: compressive strength, mean chain length (MCL), fraction r of Si in C-S-H relative to gbfs, Al/Si ratio in C-S-H silicate chains, relative fraction of Al in C-S-H, Al in octahedral (O_h) and tetrahedral (T_{d1} and T_{d2}) sites obtained from ^{27}Al BD-NMR spectra

Paste	strength [MPa]	MCL	r [%]	Al/Si (C-S-H)	Al/Si·r (relative to P7)	AlO_h [%]	AlT_d ($T_{d1}+T_{d2}$) [%]	Al(T_{d2}) (C-S-H) [%]	Al(T_{d2}) (relative to P7)
P1	32	6.9	44	0.09	0.3	53	47	12	0.5
P2	45	9.7	81	0.19	1.2	46	54	21	1.0
P3	28	6.0	62	0.15	0.7	45	55	21	1.0
P4	38	13.4	88	0.20	1.4	54	46	35	1.6
P5	30	6.0	48	0.11	0.4	76	24	5	0.2
P6	20	9.0	39	0.17	0.5	73	27	12	0.5
P7	28	6.1	64	0.20	1.0	72	22	22	1.0

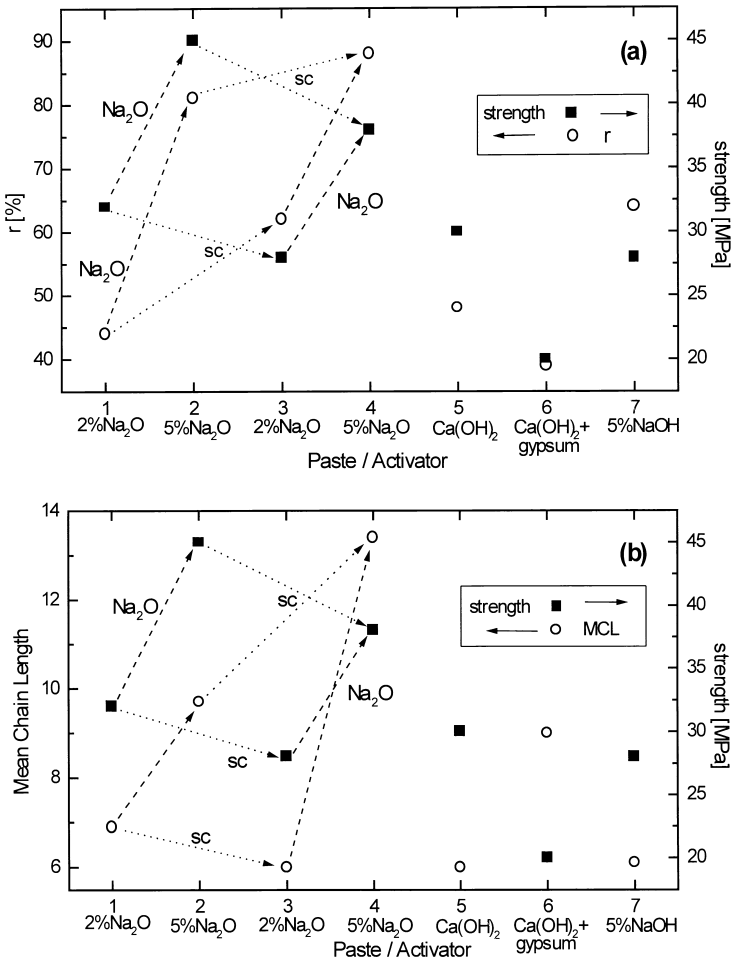

Fig. 4. Plots of (a) extent of reaction *r* and (b) mean chain length MCL of C-S-H for each hardened paste. Activator compounds and values of strength are also indicated for each case. Dotted arrows link pastes activated with increasing Na_2O concentration or cure temperature (sc: steam curing at 60°C).

formed C-S-H seems to be unaffected by the rapid precipitation of ettringite phase. On the other hand, despite P4 and P2 showing the longest chains and the highest reaction extent, no specific trend is observed between both quantities in the set of samples.

Plots of the measured Al/Si ratios versus the mean chain length MCL and the extent of reaction *r* in each sample are shown in Fig. 5a and b. As can be seen, the Al/Si content shows a slight trend to increase with *r* and MCL with the exception of pastes P1 and P5. The Al/Si ratio takes values within the range 0.15 to 0.20. In P1 and P5, even with values of *r* and MCL similar to P7, the incorporation of Al in the C-S-H phase is only half that for the other samples. Thus, the activation with $Ca(OH)_2$ or with low concentration of Na_2O/wet curing is less favorable to the incorporation of Al in the C-S-H chains. The slight increase of MCL with Al/Si is an expectable behavior considering that aluminum is able to fill the empty bridging sites giving rise to longer chains. Again, P5 and P1 appear far from the general trend, showing that in these C-S-H phases the development of the chains was done preferentially through silicon incorporation in the bridging sites.

3.2. ^{27}Al-NMR spectroscopy

^{27}Al-NMR spectra obtained from BD and CP experiments are shown in Figs. 6 and 7, respectively. The spectrum for the gbfs shows a broad resonance centered at 64.1 ppm, indicating Al located only at tetrahedral (T_d) sites (Table 5). As expected, no NMR signal was obtained through CP experiments in the gbfs sample. The spectra from hydrated pastes, however, show resonances originating from Al in T_d and octahedral (O_h) sites. For $Al(O_h)$, the CP spectra shown in Fig. 7 reveal a strong polarization transfer from ^{1}H nuclei. This fact indicates the presence of OH groups and/or water molecules coordinated around the Al atoms. Intense peaks corresponding to $Al(O_h)$ are observed at 3.5, 8.5 and 12 ppm. The peaks at 3.5 and 8.5 ppm are located in the chemical shift range of several hydrated phases, as hydrogarnets, observed in calcium aluminate cements [14]. Both lines are detectable in the spectra of all samples, though in P7 the 3.5 ppm resonance appears considerably broadened. The CP experiments show an enhancement of the relative integrated intensities $I(8.5)/I(3.5)$ with respect to BD spectra, suggesting a

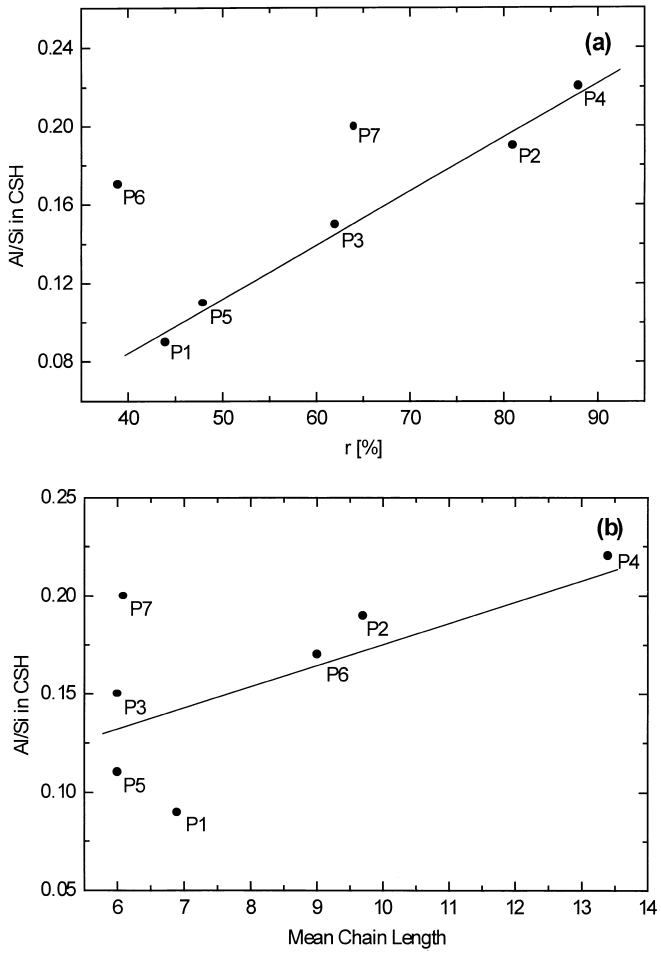

Fig. 5. Al/Si ratio in the alumino-silicate chains of C-S-H gel of each hardened paste as a function of: (a) extent of reaction *r*, calculated from the ^{29}Si-NMR spectra as the fraction of Si in C-S-H with respect to Si in unreacted gbfs, (b) the mean chain length MCL.

higher degree of OH coordination around the Al atoms associated with the 8.5 ppm line. Solely from one-dimensional ^{27}Al spectra it is difficult to assure whether these resolved peaks correspond to different Al sites or they are originated from a distribution of quadrupole coupling constants. For nuclei with spin I greater than 1/2, as aluminum ($I=5/2$), inhomogeneous broadening of the resonance line occurs due to the anisotropic nature of quadrupole interaction and also to possible spread of local electric field gradient values. So, even a phase with only one crystallographic Al-site may give rise to multiple peaks or asymmetries in the NMR spectrum, depending on the asymmetry parameter of the electric field gradient tensor and the spread of quadrupole coupling constants [15]. Nevertheless, the differential intensity enhancement observed in CP experiments support the interpretation in terms of multiple sites, and peaks at 3.5 and 8.5 ppm possibly correspond to two different hydrate phases. According to X-ray diffraction patterns these phases should be C_3AH_6 and CAH_{10}. On the other hand, as seen in Fig. 7, an additional peak appears at 12 ppm in the ^{27}Al-NMR spectrum of P6 paste. This resonance can be readily assigned to ettringite, according to X-ray diffraction data of Fig. 2. The very strong enhancement of this line by CP is an expected feature, due to the high number of coordinated water molecules/OH groups around Al in ettringite [16].

On the other hand, the T_d region of the BD spectra show two partially resolved peaks approximately at 66 and 72 ppm, say T_{d1} and T_{d2}, respectively. The T_{d2} resonance is more sharp and resolved than T_{d1}, suggesting a lower quadrupole coupling or a more ordered phase. Its chemical shift value is in agreement with the corresponding to aluminum sharing oxygen atoms with silicon. Therefore, the T_{d2} resonance may be assigned to Al in C-S-H chains. Accordingly, this resonance is better resolved in BD spectra of P7, P4 and P2, the pastes with the highest values of Al/Si in C-S-H. As seen in Fig. 7, CP is less efficient for these Al atoms as compared with Al(O_h), which is in agreement with the low number of possible attached OH groups. From the intensity of the Al(T_d) resonances, it can be noted that wet-

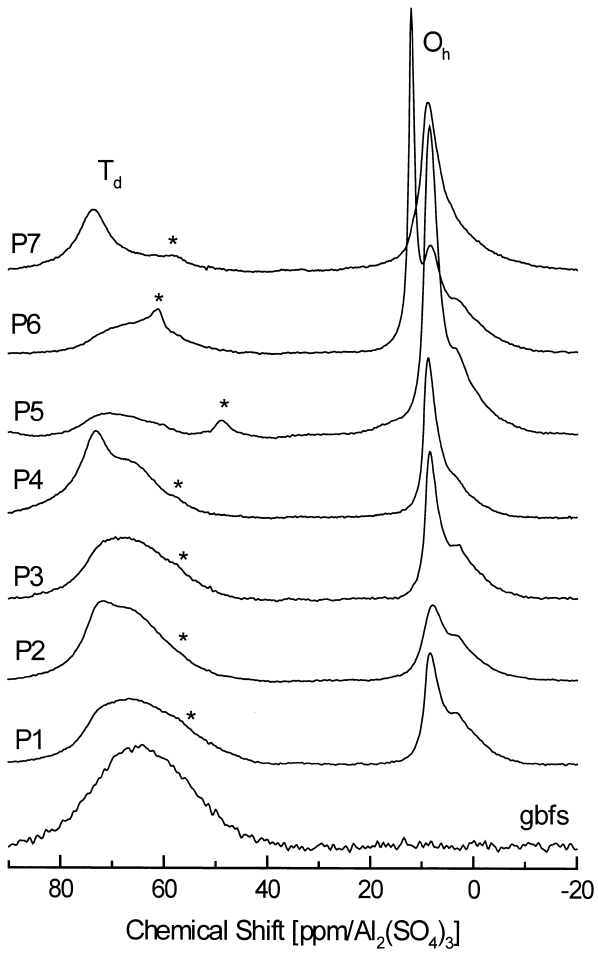

Fig. 6. ^{27}Al-BD-MAS-NMR spectra from gbfs and hydrated pastes. Resonances from Al with octahedral (O_h) and tetrahedral (T_d) coordination are indicated. Asterisks identify side bands.

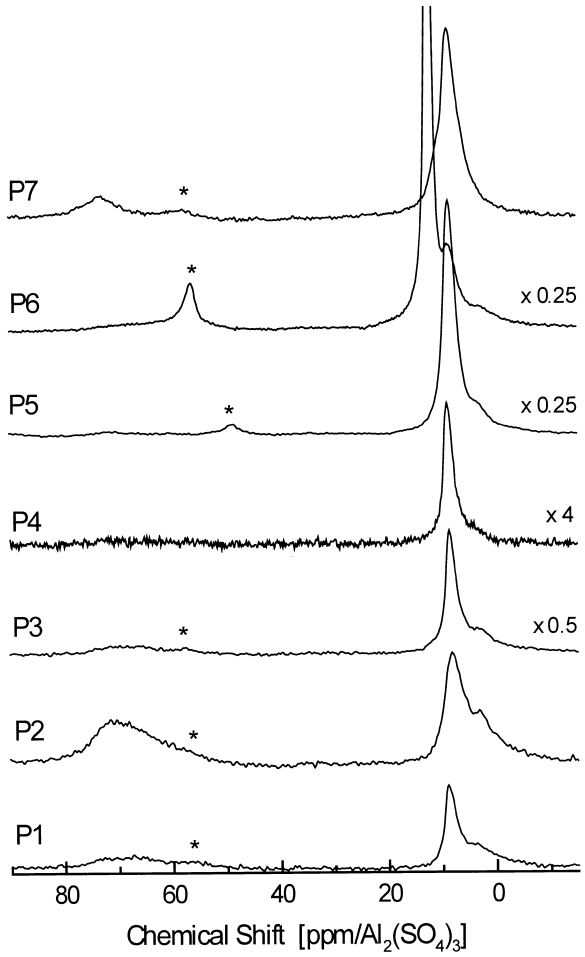

Fig. 7. $^{1}H-^{27}Al$-CP-MAS-NMR spectra from gbfs and hydrated pastes. Asterisks identify side bands.

cured (P1 and P2) and NaOH-activated (P7) pastes present the more efficient $^{1}H-^{27}Al$ polarization transfer, according to the higher concentration of water or OH groups expected in these samples.

The central position and line width of the T_{d1} peak resemble the gbfs spectrum, so it could be tentatively associated to Al in unreacted slag. Nevertheless, as seen in Fig. 7, some NMR signal can be excited by CP in the T_{d1} region of the spectrum. The efficiency of CP for each sample is equivalent to the case of the T_{d2} resonance. Such behavior is not expected for nonreacted gbfs, where there is no $^{1}H-^{27}Al$ CP signal. Then, a fraction of Al nuclei contributing to the T_{d1} peak should be participating in phases with similar degrees of hydration as those of Al in T_{d2}. Due to possible second order quadrupole broadening effects, it is difficult to associate this cross-polarizable signal with a chemical environment different from T_{d2}, as for example other Al sites in C-S-H or in another hydrated phase.

It is rather probable that the T_{d2} resonance line, from Al in C-S-H, is partially overlapped with the weak Al signal of the gbfs, in the region of -66 ppm. Due to lack of knowledge about the asymmetry of the T_{d2} line and its degree of overlap with gbfs, a reliable quantitative evaluation of the $Al(T_{d2})$ in C-S-H with respect to $Al(T_d)$ in nonhydrated gbfs could not be performed. However, a rough estimation of $Al(T_{d2})$ with respect to $Al(O_h)$ in the hydration products was done, assuming an approximate model for the deconvolution of the T_d region of ^{27}Al-BD-NMR spectra. The line for $Al(T_{d2})$ in C-S-H was approximated with a symmetric lorentzian function. A gaussian function was used to fit the T_d region around -66 ppm, which may include Al in gbfs and some fraction of Al in hydrated products. Finally, a third gaussian was used to represent the first order side band from the O_h lines (-57 to -50 ppm). Table 4 shows the relative intensities for Al resonances in the BD spectra, corresponding to O_h (hydrated phases), T_d (T_{d1}, T_{d2} and gbfs) and T_{d2} (approximate fraction for C-S-H). As can be seen from the $Al(O_h)$ column, in samples activated with Na_2O about 50% of the total aluminum belongs to hydrated phases different from C-S-H. Activation with calcium hydroxide, gypsum or NaOH raises this proportion to 75% (P5, P6, P7). These observations are in agreement with the X-ray diffraction patterns, indicating intense peaks of calcium aluminate hydrate phases in P5 and P7, and also ettringite in P6. The intensity of the deconvoluted symmetric $Al(T_{d2})$ resonance, which should give a rough estimation of Al in C-S-H, is also shown in Table 4. As can be noted, the highest intensities correspond to steam-cured alkali-activated specimens. Steam cure improves the incorporation of Al even with less alkali concentration; P2 (2%Na_2O) shows equivalent intensity to P3 (5%Na_2O). Comparing the intensities of T_{d2} in P4 and P7, it can be noted that activation with Na_2O improves the incorporation of Al in C-S-H with respect to activation with NaOH.

The product of the quantities r and Al/Si, which gives the Al content in C-S-H, is also shown in Table 4 normalized with respect to P7. Comparing these quantities with the $Al(T_{d2})$ intensities, also normalized with respect to P7 in the last column of Table 4, a reasonable agreement is found considering the uncertainty associated with the quantification of the tetrahedral region of ^{27}Al-NMR spectra. This fact reinforces the interpretation of the T_{d2} resonance as coming from Al atoms in C-S-H chains.

Table 5
Chemical shifts for the ^{27}Al resonances of gbfs and C-S-H pastes

gbfs	P1	P2	P3	P4	P5	P6	P7	Site symmetry
	3.5	3.5	3.4	3.8	3.5	3.5	–[a]	O_h
	8.3	7.7	8.3	8.6	8.5	8.3	8.6	O_h
						12		O_h
64.1	67.0	67.3	66.1	66.2	63.2	65	70	T_{d1}
	72.1	72.7	72.1	73.2	72.0	70	73.7	T_{d2}

Octahedral (O_h) and tetrahedral (T_d) sites are identified according to chemical shift values. No corrections were done to chemical shift values for quadrupole broadening.

[a] Not resolved.

4. Concluding remarks

The results obtained for the set of pastes show several similarities of the C-S-H phases obtained from activation of commercial gbfs with different compounds and cures. The connectivites of the silicate tetrahedra in all pastes, as indicated by ^{29}Si high-resolution NMR spectra, are compatible with the "dreirkette" model of C-S-H. The Al incorporation to the silicate chains occurs mainly at tetrahedra connected to Q^2 silicates, giving rise to an intense Q^2(1Al) resonance observed in all ^{29}Si-NMR spectra. Resonance lines corresponding to Q^1(1Al) were not detected. Also, it was not possible to observe any feature suggesting two chemically distinguishable Q^2(1Al) silicon species as arising from Al incorporation in bridging and nonbridging sites. These results are in agreement with previous observations in NaOH/KOH-activated gbfs pastes [7,8]. In the framework of the "dreirkette" model, as discussed by Richardson and Groves [8], values for the mean silicate-chain length MCL and the Al/Si were calculated for the set of pastes. A substantial degree of polymerization of the aluminate-silicate tetrahedra in C-S-H was observed in pastes resulting from activation with sodium silicate and gypsum/calcium hydroxide blend. The longest chains were observed in C-S-H phases resulting from activation with higher concentration of Na_2O. In pastes where hydration was partially restricted (P6), the silicates in the corresponding C-S-H phase appear as polymerized as in pastes with a higher extent of hydration (P4 or P2, for example). Activation with Na_2O and steam-curing gave the highest r values (nearly 90%). On the other hand, the activation with calcium hydroxide plus gypsum gave the lowest r value (nearly 40%), observed as a substantial amount of ettringite in the hardened paste.

Regarding the incorporation of Al to hydration products, ^{27}Al-NMR indicates that pastes activated with Na_2O (P1 to P4) show the same quantity of Al in calcium aluminate hydrate phases with respect to Al in C-S-H. In contrast, in pastes P5, P6 and P7 only 25% of observed Al belong to C-S-H phases, which indicates that more Na substitutions in Ca sites are occurring for the case of activation with Na_2O. Steam cure and higher alkali concentration enhance the incorporation of Al in C-S-H, as observed from the intensities of the T_{d2} resonances. Even with low concentration of Na_2O, through steam cure it is possible to obtain a C-S-H phase with as much aluminum as in the case of activation with higher alkali concentrations.

Acknowledgments

The authors thank Dr. Maristela Gomes da Silva for providing the samples from her PhD Thesis and Dr. Claudia Oliveira for helpful discussions and comments. Support from FAPESP (Fundação de Amparo à Pesquisa no Estado de São Paulo) is gratefully acknowledged.

References

[1] V. Agopyan, V. John, Durability evaluation on vegetable fibre reinforced materials, Build. Res. Inf. 20 (4) (1992) 233–235.
[2] D.M. Roy, I.A. Malek, Hydration of slag cement, in: S.N. Ghosh, S. Sarkar, S. Harsh (Eds.), Progress in Cement and Concrete Mineral Admixtures in Cement and Concrete, ABI Books, New Delhi, 1993, pp. 85–117.
[3] B. Talling, J. Brandstetr, Clinker-free concrete based on alkali activated slag, in: S.N. Ghosh, S. Sarkar, S. Harsh (Eds.), Progress in Cement and Concrete Mineral Admixtures in Cement and Concrete, ABI Books, New Delhi, 1993, pp. 297–341.
[4] C. Jolicoeur, M.A. Simard, T.C. To, R. Zamojska, M. Dupuis, N. Spiratos, E. Douglas, V.M. Malhotra, Chemical activation of blast-furnace slag: An overview and systematic experimental investigations, in: M. Malhotra (Ed.), Advances in Concrete Technology, CANMET, Natural Resources Canada, Ottawa, Canada, 1994, pp. 483–514.
[5] S. Wang, X.C. Pu, K.L. Scrivener, P.L. Pratt, Alkali activated slag cement and concrete: A review of its properties and problems, Adv. Cem. Res. 7 (27) (1994) 93–103.
[6] C.T. Oliveira, Pore Water in Slag Cement Pastes, PhD Thesis, EPUSP-Universidade de São Paulo, 2000.
[7] P. Schilling, L. Butler, A. Roy, H. Eaton, ^{29}Si and ^{27}Al MAS-NMR of NaOH-activated blast-furnace slag, J. Am. Ceram. Soc. 9 (1994) 2363.
[8] I.G. Richardson, G.W. Groves, The structure of the calcium silicate hydrates phases present in hardened pastes of white portland cements, J. Mater. Sci. 32 (1997) 4793.
[9] H. Morris, S. Bank, P. Ellis, ^{27}Al NMR spectroscopy of iron-bearing montmorillonite clays, J. Phys. Chem. 94 (1990) 3121.
[10] G. Engelhardt, D. Michel, High Resolution Solid-State NMR of Silicates and Zeolites, Wiley, Norwich, 1987.
[11] H.F.W. Taylor, Proposed structure for calcium silicate hydrate gel, J. Am. Ceram. Soc. 69 (1986) 464.
[12] H.F.W. Taylor, Cement Chemistry, Academic Press, New York, 1990, p. 142.
[13] I.G. Richardson, A.R. Brough, G.W. Groves, C.M. Dobson, The characterization of hardened alkali-activated blast-furnace slag pastes and the nature of the calcium silicate hydrate (C-S-H) phase, Cem. Concr. Res. 24 (1994) 813.
[14] X. Cong, R.J. Kirkpatrick, Hydration of calcium aluminate cements: A solid-state ^{27}Al NMR study, J. Am. Ceram. Soc. 76 (1993) 409.
[15] M.E. Smith, E.R.H. Van Eck, Recent advances in experimental solid state NMR methodology for half-integer spin quadrupolar nuclei, Prog. Nucl. Magn. Res. 34 (1999) 159.
[16] H.F.W. Taylor, Cement Chemistry, Academic Press, New York, 1990, p. 177.